
WHEN TASK-SPECIFIC LEARNING OUTPERFORMS TRANSFER LEARNING: A BENCHMARK OF GENE AND EXPRESSION ENCODING STRATEGIES*

Igor Sadalski

Somite.ai

Boston, MA, USA

igor.sadalski@gmail.com

ABSTRACT

Single-cell foundational models use transformer backbones that require careful engineering of gene and expression encoding strategies, yet there is no consensus on which encoding techniques are effective. We systematically compare encoding paradigms by training models from scratch under controlled conditions, evaluating them using a comprehensive evaluation suite spanning multiple evaluation dimensions: batch correction metrics (integration local inverse Simpson’s index, graph connectivity, average silhouette width), biological preservation metrics (normalized mutual information, adjusted rand index, isolated label metrics), classification performance (accuracy and macro F1), and reconstruction quality. We scale pretraining to 10 million cells across 100 diverse datasets (tenfold increase over similar studies) and compare learned versus pretrained protein model gene embeddings with four expression encoding methods (discrete binning, differentiable soft binning, logarithmic binning, and continuous encoding). Contrary to common assumptions, task-specific learned embeddings consistently outperform pretrained protein model embeddings across all metrics. The best configuration (differentiable soft binning with learned embeddings) achieves superior classification performance and substantial improvements on batch correction and biological preservation metrics. Our work provides clear empirical guidance for model design and establishes a systematic benchmark for encoding strategies in single-cell foundational models.

1 INTRODUCTION

A major goal in recent years has been to build an AI virtual cell, i.e., multi-scale, multi-modal neural network models that can represent and simulate cellular behaviour across diverse states (Bunne et al., 2024). Leading models promise to enable universal embeddings (Rosen et al., 2023), cross-species transfer (Pearce et al., 2025), multi-task transfer learning for downstream applications (Cui et al., 2024; Theodoris et al., 2023), and batch correction (Wang et al., 2021). While foundational models can be generated for different omics data types (e.g., protein, transcriptomics, tissues), here we focus on transcriptomic data. In this domain, most of the models (e.g. Cui et al. (2024); Adduri et al. (2025); Pearce et al. (2025)) use a transformer (Vaswani et al., 2017) backbone. Since transcriptomic data inherently consists of two pieces of information, gene identities and their expressions, architects of these models are faced with a design choice on how to encode this information into embeddings that transformers can process.

Different encoding strategies embody distinct assumptions about what information is most useful. For genes, it’s task-specific patterns versus biological priors; for expression values, it’s continuous precision versus discrete robustness. Figure 4 provides a schematic overview of representative encoding paradigms. For gene encoding, some models learn embeddings de novo to capture dataset-specific co-expression relationships (Cui et al., 2024), while others leverage transfer learning from pretrained protein language models such as ESM-2 (Lin et al., 2023; Adduri et al., 2025) to incorpo-

*draft in preparation for ICLR 2026, 2nd Workshop on Foundation Models for Science

rate evolutionary biological knowledge. For expression encoding, strategies range from discretizing into bins for computational efficiency (Cui et al., 2024; Gandhi et al., 2025) to using continuous or soft binning via MLPs (Pearce et al., 2025; Ho et al., 2024; Adduri et al., 2025) or applying binning based on logarithmic transformation (Wang et al., 2021).

We present a controlled benchmark that quantifies these methodologies using consistent model architecture and training procedures at a large scale. We overcome the limitations of previous work by scaling up the pretraining data tenfold to 10 million cells, increasing dataset diversity by using 100 different datasets, introducing new tokenization strategies such as log binning and raw embedding, and performing evaluation against the Tabula Sapiens v2 benchmark.

The main contributions of this work are:

- **A comprehensive evaluation suite** spanning batch correction, biological preservation, classification, and reconstruction metrics across 26 diverse tissue datasets.
- **A tenfold increase in scale of pretraining data** to 10 million cells across 100 diverse datasets.
- **A systematic evaluation of encoding strategies** comparing learned versus pretrained protein model gene embeddings and four expression encoding methods (discrete binning, differentiable soft binning, logarithmic binning, and continuous encoding) under controlled conditions with consistent model architecture and training procedures.

2 RELATED WORK

Limited scientific literature has addressed this problem. Most benchmarking efforts have focused on evaluating downstream applications, such as perturbation prediction (Ahlmann-Eltze et al., 2024; Wenteler et al., 2024), using already pretrained models. In this work, we focus more on specific architectural choices and pretrain our models from scratch. A similar approach was taken in HEIMDALL (Haber et al., 2025), a modular tokenization framework, where authors tried to evaluate different encoding strategies. However, they pretrained their transformer model on only a few datasets with a total of 1 million cells. This limited scale and dataset diversity likely prevents transformers from learning robust, generalizable representations, as transformer performance scales with training data size (Kaplan et al., 2020). In comparison, regular transformer models in the field are trained on, e.g., 266 million cells (Gandhi et al., 2025) and hundreds of diverse datasets. Given improved transformer performance with data scale (Kaplan et al., 2020), we scale our pretraining to better align with the field’s standard practices.

3 METHODS

3.1 MODEL ARCHITECTURE AND PRETRAINING

We represented cells as bags of gene-expression pairs. Each cell i contains M_i genes with non-zero expression values, represented as a sequence of gene-expression pairs:

$$\mathcal{C}_i = ((g_{i,1}, x_{i,1}), \dots, (g_{i,M_i}, x_{i,M_i})) \quad (1)$$

where $g_{i,j}$ denotes the j -th gene identifier and $x_{i,j}$ denotes its corresponding expression value in cell i .

Prior to encoding, we normalized expression values for each cell to a constant total c_{norm} and applied log1p transformation:

$$\tilde{x}_{i,j} = \log \left(1 + \frac{x_{i,j}}{\sum_{k=1}^{M_i} x_{i,k}} \times c_{\text{norm}} \right) \quad (2)$$

where M_i is the number of genes in cell i , c_{norm} is a normalization constant (typically 10^4 or 10^6), and k indexes over all genes in cell i . This normalization step ensures consistent scaling across cells with varying sequencing depths.

Because transformers scale with the square of the size of the context window (number of inputs), we employed a sampling strategy to select a subset of genes for each cell. Let $S : \mathcal{C}_i \rightarrow$

$\{(g_{i,j}, x_{i,j})\}_{j=1}^K$ be a sampling function that takes cell i and returns K gene-expression pairs, where $K = \min(\text{context_window}, M_i)$. During training, for datasets where the number of non-zero expressed genes exceeded the context window, we randomly sampled K genes from all non-zero expressed genes in each cell:

$$\mathcal{S}_{\text{random}}^{(i)} = \text{RandomSample}(\{g_j : x_{i,j} > 0\}, K) \quad (3)$$

This approach ensures diverse gene representation across training examples while maintaining computational feasibility for large gene vocabularies.

The training objective was to predict masked expression values given the gene identities and unmasked expression context. To this end, we first computed embeddings for both gene identities and expression values. The gene embedding for each gene was obtained as:

$$\mathbf{e}_g^{(i,j)} = \text{enc}_g(g_{i,j}) \in \mathbb{R}^{d_g}, \quad (4)$$

where enc_g is the gene encoding function (detailed in Section 3.2), d_g is the gene embedding dimension, and $\mathbf{e}_g^{(i,j)} \in \mathbb{R}^{d_g}$ is the gene embedding vector. For expression values, we randomly masked a fraction p_{mask} of gene-expression pairs during training. The expression embedding was computed as:

$$\mathbf{e}_x^{(i,j)} = \begin{cases} \text{enc}_x(\tilde{x}_{i,j}) & \text{with probability } 1 - p_{\text{mask}} \\ \mathbf{m} & \text{with probability } p_{\text{mask}} \end{cases} \quad (5)$$

where enc_x is the expression encoding function (detailed in Section 3.3), $\mathbf{e}_x^{(i,j)} \in \mathbb{R}^{d_x}$ is the expression embedding vector, p_{mask} is the masking probability, and $\mathbf{m} \in \mathbb{R}^{d_x}$ is a learnable mask token with dimension d_x matching the expression embedding dimension.

The combined gene-expression embedding for the j -th gene in cell i is obtained by summing the gene and expression embeddings:

$$\mathbf{z}_0^{(i,j)} = \mathbf{e}_g^{(i,j)} + \mathbf{e}_x^{(i,j)} \quad (6)$$

where $\mathbf{z}_0^{(i,j)} \in \mathbb{R}^d$ is the combined embedding for gene j in cell i , and d is the model dimension (equal to both d_g and d_x). The combined embeddings for all K genes in cell i are concatenated together to form the input sequence for the model:

$$\mathbf{z}_0^{(i)} = [\mathbf{z}_0^{(i,1)}, \dots, \mathbf{z}_0^{(i,K)}] \quad (7)$$

where $\mathbf{z}_0^{(i)} \in \mathbb{R}^{K \times d}$ is the input sequence for cell i containing K gene embeddings. These combined embeddings were then passed through a transformer encoder. Grouping the gene-embeddings per cell and recursively applying the transformer layers, we obtained:

$$\mathbf{z}_l^{(i)} = f_{\text{transformer}}(\mathbf{z}_{l-1}^{(i)}) \quad (8)$$

where $f_{\text{transformer}}$ denotes a standard transformer encoder layer, $l \in \{1, \dots, n\}$ indexes the layers, and n is the total number of transformer layers.

The predicted expression value for the j -th gene in cell i is decoded from the final transformer layer output using a simple MLP:

$$\bar{x}_{i,j} = \text{MLP}(\mathbf{z}_n^{(i,j)}) \quad (9)$$

where $\mathbf{z}_n^{(i,j)} \in \mathbb{R}^d$ is the output embedding for gene j in cell i from the final transformer layer, and $\bar{x}_{i,j} \in \mathbb{R}$ is the predicted expression value. We optimized the model using mean squared error loss for reconstruction of masked gene expression values (Wang et al., 2021; Adduri et al., 2025; Ho et al., 2024; Cui et al., 2024):

$$\mathcal{L}_{i,j} = \frac{1}{|\mathcal{U}_{\text{unk}}|} \sum_{j \in \mathcal{U}_{\text{unk}}} (\tilde{x}_{i,j} - \bar{x}_{i,j})^2 \quad (10)$$

where $\mathcal{L}_{i,j}$ is the loss for gene j in cell i , \mathcal{U}_{unk} represents the set of masked gene indices, $\tilde{x}_{i,j}$ is the normalized true expression value, and $\bar{x}_{i,j}$ is the predicted expression value from Equation 9.

3.2 GENE ENCODING STRATEGIES

Learned encoding is obtained by passing the gene identifier through a learned embedding table (Cui et al., 2024; Gandhi et al., 2025). This approach allows the model to generate task-specific representations for each gene, enabling it to capture dataset-specific relationships.

$$\text{enc}_g^{\text{learned}}(g_{i,j}) = \text{Embedding}(g_{i,j}) \quad (11)$$

ESM-2 encoding uses precomputed embeddings retrieved from the ESM-2 (3B) model dictionary (Lin et al., 2023). STATE (Adduri et al., 2025) leverages this approach, using large pretrained protein language models to provide biologically-informed representations that are consistent across datasets and species, making it a strong choice for transfer learning and handling new or rare gene symbols. We projected these embeddings through an MLP to match the model dimension.

$$\text{enc}_g^{\text{ESM-2}}(g_{i,j}) = \text{MLP}(\mathcal{E}(g_{i,j})) \quad (12)$$

where $\mathcal{E}(g_{i,j})$ denotes the precomputed ESM-2 embedding for gene identifier $g_{i,j}$, and MLP is a multi-layer perceptron that projects the embedding to the model dimension.

3.3 EXPRESSION ENCODING STRATEGIES

Raw expression encoding uses a simple MLP on normalized data. This approach preserves the full, continuous information from the expression measurement and is the most direct way to encode quantitative gene expression levels.

$$\text{enc}_x^{\text{raw}}(\tilde{x}_{i,j}) = \text{MLP}(\tilde{x}_{i,j}) \quad (13)$$

Hard binning encoding discretizes expression values into bins. This method groups expression levels into discrete intervals, trading off resolution for robustness and simplifying the input space (Cui et al., 2024; Gandhi et al., 2025).

$$b_{i,j} = \begin{cases} k, & \text{if } x_{i,j} > 0 \text{ and } x_{i,j} \in [\beta_k, \beta_{k+1}], \\ 0, & \text{if } x_{i,j} = 0, \end{cases} \quad (14)$$

where $b_{i,j}$ is the bin index for the expression value of gene j in cell i , k is the bin index, and β_k and β_{k+1} are the lower and upper boundaries of bin k , respectively. Expression embedding is obtained using an embedding layer:

$$\text{enc}_x^{\text{hard bin}}(x_{i,j}) = \text{Embedding}(b_{i,j}) \quad (15)$$

Log binning encoding compresses a wide dynamic range of expression values using a logarithmic transformation before discretizing. This approach can potentially mitigate the effects of outliers or skewed distributions. STATE (Adduri et al., 2025) uses this approach with ESM-2 embeddings, while scBERT (Wang et al., 2021) employs log binning with discrete tokenization.

$$b_{i,j} = \min(\lfloor \log_2(x_{i,j} + 1) \rfloor, B_{\max}) \quad (16)$$

where $b_{i,j}$ is the bin index for the expression value of gene j in cell i , and B_{\max} is the maximum bin index. Bins are embedded using an embedding layer:

$$\text{enc}_x^{\text{log bin}}(x_{i,j}) = \text{Embedding}(b_{i,j}) \quad (17)$$

Soft binning encoding uses a softmax over potential bins to allow fractional/bin-weighted expression, which can capture uncertainty and subtle intensity differences between expression values, making the encoding differentiable and potentially more expressive (Ho et al., 2024; Hao et al., 2024; Pearce et al., 2025).

$$\boldsymbol{\alpha}_x^{(i,j)} = \text{Softmax}(\mathbf{W}_{x,2} \text{LeakyReLU}(\mathbf{W}_{x,1} x_{i,j})) \quad (18)$$

where $\boldsymbol{\alpha}_x^{(i,j)}$ is a vector of bin weights for the expression value of gene j in cell i , $\mathbf{W}_{x,1}$ and $\mathbf{W}_{x,2}$ are learnable weight matrices, and LeakyReLU is the LeakyReLU activation function. The expression embedding is obtained by performing a soft lookup in the embedding table:

$$\text{enc}_x^{\text{soft bin}}(x_{i,j}) = \sum_{k=1}^b \alpha_{x,k}^{(i,j)} \mathbf{T}_k \quad (19)$$

where b is the number of bins, $\alpha_{x,k}^{(i,j)}$ is the k -th element of $\boldsymbol{\alpha}_x^{(i,j)}$, and \mathbf{T}_k is the k -th embedding vector in the embedding table \mathbf{T} .

4 EXPERIMENTS

4.1 TRAINING

We trained our models on 101 diverse single-cell RNA sequencing datasets comprising over 10 million cells, randomly selected from the curated collection used to train the Transcriptformer model (Pearce et al., 2025). The datasets span diverse tissue types, experimental protocols, species, biological conditions, developmental stages, and disease states (see Appendix A). We evaluated four different expression encoding strategies and two different gene encoding strategies by training models for all combinations of these strategies (8 models total). During the training process we used the hyperparameters defined in Table 1 in the Appendix, which were based on previous works (Cui et al., 2024; Adduri et al., 2025; Pearce et al., 2025). All models were trained using automatic mixed precision (AMP) with FP16 to accelerate training. During training, we recorded the reconstruction loss for each model using Mean Squared Error on masked gene expression values, which directly measures the model’s ability to predict masked expression values during pretraining. We recorded the best model checkpoints based on the validation reconstruction loss.

4.2 EVALUATION

We evaluated all models on 26 tissue-specific datasets from the Tabula Sapiens v2 benchmark (Tabula Sapiens Consortium et al., 2022), comprising more than half a million cells across diverse human tissues. This benchmark represents a standard evaluation protocol in the field and has been used to evaluate other foundational models (Pearce et al., 2025). Using each trained model, we embedded 26 datasets that constituted the evaluation dataset. For each embedded evaluation dataset, we generated cell embeddings by extracting token embeddings from the final encoder layer (where each token represents a gene-expression pair) and mean-pooling these embeddings across all valid (non-padded) positions for each cell. Our embeddings were annotated with cell type. Additionally, for the batch key we used the `10X_run` identifier, which distinguishes cells from different 10X Genomics sequencing runs.

Batch correction metrics. To assess batch effect removal, we used the scib package (Luecken et al., 2022) and computed: Integration Local Inverse Simpson’s Index, which measures the diversity of batch labels in the local neighborhood of each cell to quantify batch mixing; Cell-type Local Inverse Simpson’s Index, which evaluates the preservation of biological structure by measuring the diversity of cell-type labels in the local neighborhood; Average Silhouette Width for batch, which measures how well batches are mixed globally using average silhouette width; and graph connectivity, which assesses whether cells sharing the same label form a fully connected subgraph in the k-nearest neighbors graph.

Biological preservation metrics. Similarly to batch correction metrics (also using the scib package (Luecken et al., 2022)), we computed: Average Silhouette Width for label, which quantifies how well cells of the same cell type cluster together using average silhouette width computed over cell-type labels; Normalized Mutual Information, which measures the normalized mutual information between predicted clusters and true cell-type labels; Adjusted Rand Index, which computes the adjusted rand index between predicted clusters and true cell-type labels; isolated label F1 score, which evaluates the F1 score for cell types that are isolated in the embedding space; and isolated label silhouette, which measures the silhouette score for isolated cell types.

Cell type classification. To compute cell type classification performance, we extracted cell embeddings by mean-pooling token embeddings from the final encoder layer (where each token represents a gene-expression pair) (Pearce et al., 2025). We filtered out cells with missing cell type annotations and removed cell types with fewer than 250 cells to ensure robust evaluation. We split the data into training and test sets using an 80/20 stratified split. We trained a k-nearest neighbors classifier with $k = 10$ on the training set and evaluated performance on the held-out test set.

5 RESULTS

We evaluated all 8 model configurations (2 gene encoding strategies \times 4 expression encoding strategies) on 26 tissue-specific datasets from the Tabula Sapiens v2 benchmark. For each encoder config-

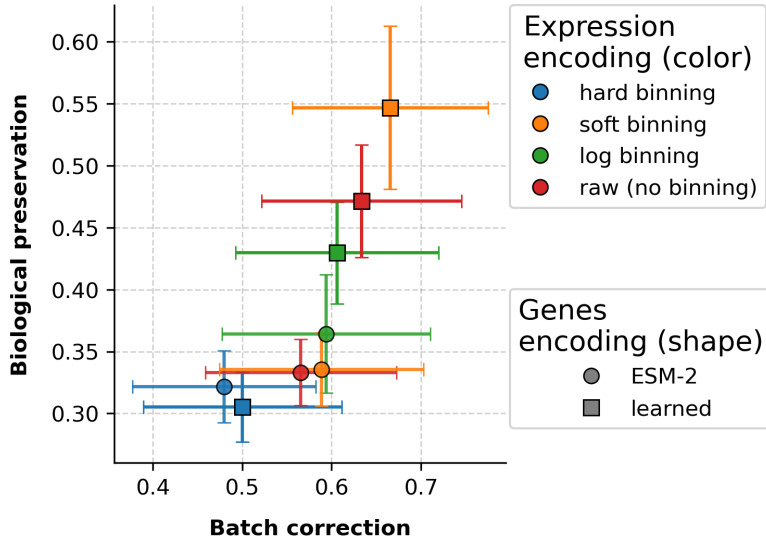


Figure 1: Performance comparison across encoding strategies on batch correction and biological preservation metrics. To obtain a single point, first, we take one of the evaluation datasets (we subset 11 out of 26 datasets). For that dataset we compute several evaluation metrics, then averaged those metrics within the dataset to obtain a per-dataset mean for each model configuration. Next, we aggregated results by taking the mean and standard deviation of these per-dataset metric means across all datasets (so error bars are standard deviations of the per-dataset means). The X-axis shows batch removal performance, which is the average of metrics related to batch correction (Integration Local Inverse Simpson’s Index, graph connectivity, Average Silhouette Width for batch). The Y-axis shows biology conservation performance, which is the average of metrics that capture biological signal preservation (Average Silhouette Width for label, Cell-type Local Inverse Simpson’s Index, Normalized Mutual Information, Adjusted Rand Index, isolated label F1 score, isolated label silhouette score). Colors distinguish expression encoding strategies (hard binning, soft binning, log binning, raw expression), and marker shapes indicate gene encoding strategies (learned embedding or ESM-2 embedding).

uration, we embedded separately each of the 26 datasets and then computed selected metrics from the scib package (Luecken et al., 2022) which are used to evaluate batch correction and biological preservation, cell type classification performance, and pretraining reconstruction loss. Our evaluation revealed three key findings: (1) learned gene embeddings substantially outperformed ESM-2 embeddings across all metrics, (2) soft binning emerged as the optimal expression encoding strategy, and (3) pretraining reconstruction quality correlated with downstream task performance.

5.1 BATCH CORRECTION AND BIOLOGICAL PRESERVATION

Figure 1 shows a comparison of the trained models’ ability to perform batch correction and preserve biological features. Each point summarizes the model’s average batch correction (average of selected metrics) and biological preservation (average of selected metrics) performance aggregated across datasets. In these results, learned gene embeddings with soft binning achieve the best performance, representing a 16% improvement over the second-best configuration (raw encoding with learned embeddings at 0.471). Overall, learned gene embeddings provide a 29% relative improvement over ESM-2 embeddings on the combined metrics, supporting the advantage of using task-specific learned representations for both batch correction and biological signal conservation. The batch correction metrics show high variability, with an average coefficient of variation of 29% (mean standard deviation 0.11 over mean score 0.38), reflecting substantial differences across the 26 evaluation datasets.

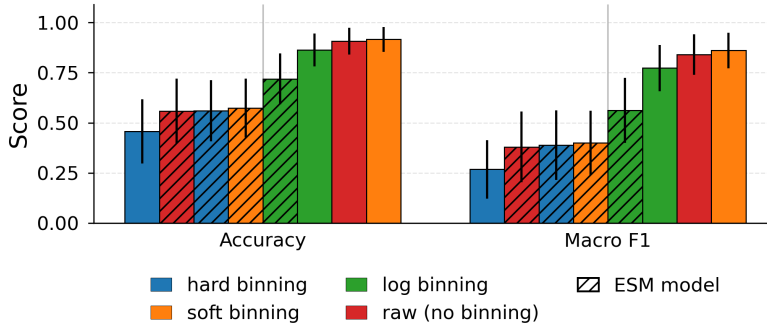


Figure 2: Cell type classification performance across encoding strategies. Bars show mean accuracy and macro F1 score with error bars indicating standard deviation across 26 evaluation datasets. Colors indicate expression encoding strategies (hard, soft, log, raw); hatching (///) indicates ESM-2 gene encoding. Configurations are sorted in ascending order.

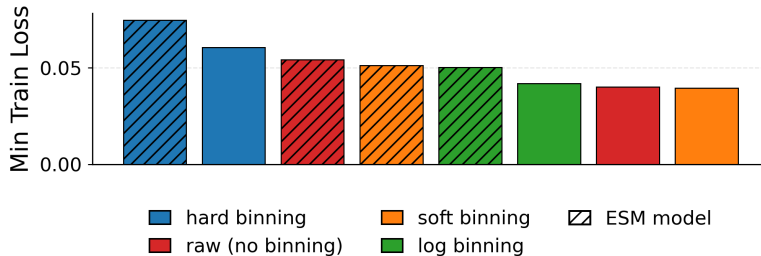


Figure 3: Minimum Mean Squared Error (MSE) training loss achieved during pretraining for each model configuration. Bars are sorted by minimum loss in descending order. Colors indicate expression encoding strategies (hard, soft, log, raw); hatching (///) indicates ESM-2 gene encoding.

5.2 CELL TYPE CLASSIFICATION PERFORMANCE

Figure 2 shows cell type classification performance across all encoding configurations. Learned gene embeddings outperform ESM-2 embeddings for three out of four cases, achieving 30% higher accuracy and 58% higher macro F1 score on average. The best-performing configuration combines learned gene embeddings with soft binning, achieving 91.6% accuracy and 86.0% macro F1 score. This represents a 92% improvement in macro F1 over hard binning with learned embeddings (44.8% macro F1). The consistent advantage of learned embeddings across all expression encoding strategies suggests that task-specific representations capture more relevant information for transcriptomic tasks than transfer learning from protein language models. Furthermore, the order of performance for different methods, in both accuracy and macro F1, is mostly consistent with other results ??.

5.3 PRETRAINING RECONSTRUCTION QUALITY

Figure 3 shows the minimum training reconstruction loss achieved during pretraining for each model configuration. Configurations with learned gene embeddings achieve lower minimum training loss than ESM-2 configurations (0.046 vs 0.058 MSE on average, 21% improvement), aligning with downstream performance. This correlation suggests that better pretraining reconstruction quality translates to improved downstream task performance. The higher training loss for ESM-2 configurations, combined with observed training instability (loss diverging in all four ESM-2 cases and learned hard binning), indicates that transfer learning from protein language models may introduce optimization challenges that limit effectiveness for transcriptomic tasks.

6 DISCUSSION

Learned gene embeddings outperform ESM-2 encoding. Despite an MLP layer projecting ESM-2 embeddings to the model dimension, models trained with ESM-2 embeddings showed unstable training with loss diverging in all four cases. Learned embeddings achieved an average 39% relative improvement over ESM-2 embeddings across all metrics. This gap suggests that task-specific representations captured dataset-specific co-expression relationships more relevant for transcriptomic tasks than evolutionary protein-level information. Additionally, single-cell data includes many non-coding genes, pseudogenes, and gene isoforms not well-represented in protein language models.

Soft binning provides optimal expression encoding. Soft binning balances discrete and continuous representations. When combined with learned gene embeddings, it achieved 91.6% classification accuracy and 86.0% macro F1 score, with a 41% improvement on batch integration and biological preservation metrics and 92% improvement on macro F1 over hard binning. Unlike hard binning, soft binning preserved information at bin boundaries and captured subtle expression differences, while providing regularization that may help learn more robust representations than raw continuous encoding.

Our evaluation is limited to human tissues, cell type classification, and a single model architecture. Future work should evaluate additional downstream tasks and species, investigate alternative architectures, and provide mechanistic insights into why learned embeddings and soft binning outperform their alternatives.

7 CONCLUSION

We present a large-scale systematic benchmark comparing gene and expression encoding strategies, training 8 configurations on over 10 million cells across 100 diverse datasets under controlled conditions. We evaluate all configurations using a comprehensive evaluation suite spanning batch correction, biological preservation, classification, and reconstruction metrics across 26 diverse tissue datasets. Our evaluation yields three key findings: (1) task-specific learned gene embeddings substantially outperform pretrained protein model embeddings, achieving 39% average improvement across all metrics; (2) differentiable soft binning emerges as the optimal expression encoding strategy when combined with learned embeddings, achieving 91.6% classification accuracy and 86.0% macro F1 score; (3) gene encoding choice has greater impact than expression encoding choice, with learned embeddings providing consistent improvements across all expression encoding strategies. This benchmark establishes clear empirical guidance for model design decisions and provides reproducible results for future method development.

IMPACT STATEMENT

This paper presents a benchmark study that provides empirical guidance for designing effective foundational models in single-cell RNA sequencing analysis. Potential positive impacts include enabling more effective analysis tools for biomedical research and providing reproducible benchmarks for method comparison. Potential negative impacts are limited, as this is a methodological study focused on model architecture rather than direct applications.

ACKNOWLEDGEMENTS

We thank Somite AI for their help and guidance throughout this work.

REFERENCES

Abhinav K Adduri, Dhruv Gautam, Beatrice Bevilacqua, Alishba Imran, Rohan Shah, Mohsen Naghipourfar, Noam Teyssier, Rajesh Ilango, Sanjay Nagaraj, Mingze Dong, Chiara Ricci-Tam, Christopher Carpenter, Vishvak Subramanyam, Aidan Winters, Sravya Tirukkovaular, Jeremy Sullivan, Brian S Plosky, Basak Eraslan, Nicholas D Youngblut, Jure Leskovec, Luke A Gilbert, Silvana Konermann, Patrick D Hsu, Alexander Dobin, Dave P Burke, Hani Goodarzi, and Yusuf H

-
- Roohani. Predicting cellular responses to perturbation across diverse contexts with state. *bioRxiv*, 2025. doi: 10.1101/2025.06.26.661135. URL <https://doi.org/10.1101/2025.06.26.661135>. Preprint.
- Constantin Ahlmann-Eltze, Wolfgang Huber, and Simon Anders. Deep learning-based predictions of gene perturbation effects do not yet outperform simple linear methods. *Nature Methods*, 2024. doi: 10.1038/s41592-025-02772-6. URL <https://doi.org/10.1038/s41592-025-02772-6>. Published version.
- Charlotte Bunne, Yusuf Roohani, Yanay Rosen, others, Emma Lundberg, Jure Leskovec, and Stephen R Quake. How to build the virtual cell with artificial intelligence: Priorities and opportunities. *Cell*, 187(25), 2024.
- Haotian Cui, Chloe Wang, Hassaan Maan, Kuan Pang, Fengning Luo, Nan Duan, and Bo Wang. scgpt: toward building a foundation model for single-cell multi-omics using generative ai. *Nature Methods*, 21:1–12, 2024. doi: 10.1038/s41592-024-02201-0. URL <https://doi.org/10.1038/s41592-024-02201-0>.
- Shreshth Gandhi, Farnoosh Javadi, Valentine Svensson, Umair Khan, Matthew G. Jones, John Yu, Daniele Merico, Hani Goodarzi, and Nima Alidoust. Tahoe-x1: Scaling perturbation-trained single-cell foundation models to 3 billion parameters. *bioRxiv*, 2025. doi: 10.1101/2025.10.23.683759. URL <https://doi.org/10.1101/2025.10.23.683759>. Preprint.
- Ellie Haber, Shahul Alam, Nicholas Ho, Renming Liu, Evan Trop, Shaoheng Liang, Muyu Yang, Spencer Krieger, and Jian Ma. Heimdall: A modular framework for tokenization in single-cell foundation models. *bioRxiv*, pp. 2025–11, 2025.
- M. Hao, J. Gong, X. Zeng, et al. Large-scale foundation model on single-cell transcriptomics. *Nature Methods*, 21:1481–1491, 2024. doi: 10.1038/s41592-024-02305-7. URL <https://doi.org/10.1038/s41592-024-02305-7>.
- Nicholas Ho, Caleb N Ellington, Jinyu Hou, Sohan Addagudi, Shentong Mo, Tianhua Tao, Dian Li, Yonghao Zhuang, Hongyi Wang, Xingyi Cheng, Le Song, and Eric P Xing. Scaling dense representations for single cell with transcriptome-scale context. *bioRxiv*, 2024. doi: 10.1101/2024.11.28.625303. URL <https://doi.org/10.1101/2024.11.28.625303>. Preprint.
- Jared Kaplan, Sam McCandlish, Tom Henighan, Tom B. Brown, Benjamin Chess, Rewon Child, Scott Gray, Alec Radford, Jeffrey Wu, and Dario Amodei. Scaling laws for neural language models. *arXiv preprint arXiv:2001.08361*, 2020. URL <https://arxiv.org/abs/2001.08361>. Preprint.
- Zeming Lin, Halil Akin, Roshan Rao, Brian Hie, Zhongkai Zhu, Wenting Lu, Nikita Smetanin, Robert Verkuil, Ori Kabeli, Yaron Shmueli, Allan dos Santos Costa, Maryam Fazel-Zarandi, Tom Sercu, Salvatore Candido, and Alexander Rives. Evolutionary-scale prediction of protein structure from sequence. *Nature*, 622(7983):827–835, 2023. doi: 10.1038/s41586-023-06520-w. URL <https://doi.org/10.1038/s41586-023-06520-w>.
- Malte D. Luecken, M. Büttner, K. Chaichoompu, A. Danese, M. Interlandi, M. F. Mueller, D. C. Strobl, L. Zappia, M. Dugas, M. Colomé-Tatché, and Fabian J. Theis. Benchmarking atlas-level data integration in single-cell genomics. *Nature Methods*, 19:41–50, 2022. doi: 10.1038/s41592-021-01336-8. URL <https://doi.org/10.1038/s41592-021-01336-8>.
- James D Pearce, Sara E Simmonds, Gita Mahmoudabadi, Lakshmi Krishnan, Giovanni Palla, Ana-Maria Istrate, Alexander Tarashansky, Benjamin Nelson, Omar Valenzuela, Donghui Li, Stephen R Quake, and Theofanis Karaletsos. A cross-species generative cell atlas across 1.5 billion years of evolution: The transcriptformer single-cell model. *bioRxiv*, 2025. doi: 10.1101/2025.04.25.650731. URL <https://doi.org/10.1101/2025.04.25.650731>. Preprint.
- Yanay Rosen, Yusuf Roohani, Ayush Agarwal, Leon Samotorčan, Tabula Sapiens Consortium, Stephen R Quake, and Jure Leskovec. Universal cell embeddings: A foundation model for cell biology. *bioRxiv*, 2023. doi: 10.1101/2023.11.28.568918. URL <https://doi.org/10.1101/2023.11.28.568918>. Preprint.

Tabula Sapiens Consortium, Robert C Jones, Jim Karkanias, Mark A Krasnow, Angela Oliveira Pisco, Stephen R Quake, Julia Salzman, Nir Yosef, Bryan Bulthaup, Phillip Brown, Will Harper, Michael Hemenez, Ravikumar Ponnusamy, Ahmad Salehi, Bhavani A Sanagavarapu, Eileen Spallino, Kalleen A Aaron, Waldo Concepcion, James M Gardner, Brendan Kelly, Nicholas Neidlinger, Zifa Wang, Sheela Crasta, Saroja Kolluru, Maurizio Morri, Yan Tan, Kyle J Travaglini, Chenling Xu, Maria Alimova, Nicholas E Banovich, Ben A Barres, Philip A Beachy, Biter Bilen, Douglas Brownfield, Charles K F Chan, Songming Chen, Michael F Clarke, Sabrina D Conley, Spyros Darmanis, Aaron Demers, Kubilay Demir, Antoine de Morree, Tony Divita, Haley du Bois, Hamid Ebadi, F Hernan Espinoza, Matt Fish, Qiang Gan, Benson M George, Jeffrey M Granja, Foad Green, Gunsagar S Gulati, Michael S Haney, Julie A Harris, Yanzhe He, Shayan Hosseinzadeh, Albin Huang, Kerwyn Casey Huang, Atsushi Iriki, Eric Jean, Kevin S Kao, Guruswamy Karnam, Aaron M Kershner, Bernhard M Kiss, William Kong, Maya E Kumar, Jonathan Lam, Song E Lee, Benoit Lehallier, Qiang Li, Yan Li, Ling Liu, Annie Lo, Wan-Jin Lu, Marisol F Lugo-Fagundo, Anjali Manjunath, Andrew P May, Ashley Maynard, Aaron McGeever, Madeleine McKay, Michael I Miller, Mais Moussa, Ravi Mylvaganam, EK Neumann, Joseph Noh, Roel Nusse, Irene Papatheodorou, Traci Peng, Lolita Penland, Katherine Pollard, Robert Puccinelli, Zhen Qi, Stephen R Quake, Thomas A Rando, Micha Sam Raredon, Karine Rizzoti, Katherine Rogers, Yanay Rosen, M Elizabeth Rothenberg, Meritxell Rovira, Yaroslava Ruzankina, Nicholas Schaum, Eran Segal, Jun Seita, Rahul Sinha, Rene V Sit, Justin Sonnenburg, Christof Stringer, Kai Tan, Michelle Tan, Sudhir Gopal Tattikota, Kyle J Travaglini, Carolina Tropini, Michelle Tsui, Lucas Waldburger, Bruce M Wang, Linda J van Weele, Brice M Weinstein, Michael N Wosczyna, Angela Wu, Jinyi Xiang, Sizun Xue, Kevin A Yamauchi, Andrew C Yang, Lakshmi P Yerra, Justin Youngyunipatkul, Bo Yu, Fabio Zanini, Gizem Zardeneta, Tiffany Zee, Chunyu Zhao, Fan Zhang, Hui Zhang, Martin JinYe Zhang, Lu Zhou, and Daniel R Zollinger. The tabula sapiens: A multiple-organ, single-cell transcriptomic atlas of humans. *Science*, 376(6594):eabl4896, 2022. doi: 10.1126/science.abl4896. URL <https://doi.org/10.1126/science.abl4896>.

Christina V Theodoris, Ling Xiao, Anant Chopra, Mark D Chaffin, Zeina R Al Sayed, Matthew C Hill, Helene Mantineo, Elizabeth M Brydon, Zexian Zeng, X. Shirley Liu, and Patrick T Ellinor. Transfer learning enables predictions in network biology. *Nature*, 618(7965):616–624, 2023. doi: 10.1038/s41586-023-06139-9. URL <https://doi.org/10.1038/s41586-023-06139-9>.

Ashish Vaswani, Noam Shazeer, Niki Parmar, Jakob Uszkoreit, Llion Jones, Aidan N Gomez, Łukasz Kaiser, and Illia Polosukhin. Attention is all you need. *Advances in Neural Information Processing Systems*, 30, 2017. URL <https://proceedings.neurips.cc/paper/2017/file/3f5ee243547dee91fb053c1c4a845aa-Paper.pdf>.

Wenchuan Wang, Fan Yang, Yuan Fang, Duyu Tang, Junzhou Huang, Hui Lu, and Jianhua Yao. scbert: a large-scale pretrained deep language model for cell type annotation of single-cell rna-seq data. *bioRxiv*, 2021. doi: 10.1101/2021.12.05.471261. URL <https://doi.org/10.1101/2021.12.05.471261>. Preprint.

A. Wenteler, M. Occhetta, N. Branson, M. Huebner, V. Curean, W. T. Dee, W. T. Connell, A. Hawkins-Hooker, S. P. Chung, Y. Ektefaie, A. Gallagher-Syed, and C. M. V. Córdova. Perteval-scfm: Benchmarking single-cell foundation models for perturbation effect prediction. *bioRxiv*, 2024. doi: 10.1101/2024.10.02.616248. URL <https://doi.org/10.1101/2024.10.02.616248>. Preprint.

A ADDITIONAL DETAILS

A.1 REPRODUCIBILITY

Training datasets are from publicly available sources (Pearce et al., 2025). Evaluation datasets from Tabula Sapiens v2 are available from the official repository (Tabula Sapiens Consortium et al., 2022).

Table 1: Hyperparameters used for model training.

Hyperparameter	Value
<i>Model Architecture</i>	
Model dimension (d_{model})	512
Number of transformer blocks (n_{blocks})	12
Number of attention heads (n_{head})	8
Feed-forward dimension (d_{hid})	1024
Dropout	0.1
Context window	1024
<i>Training</i>	
Batch size	512
Gradient accumulation steps	32
Effective batch size	16,384
Epochs	3
Learning rate	3×10^{-4}
Weight decay	10^{-5}
Optimizer betas	[0.9, 0.95]
Max gradient norm	1.0
Scheduler	Cosine annealing
Warmup steps	2000
Early stopping patience	100
<i>Data</i>	
Validation ratio	0.001
Test ratio	0.001
Masking probability (p_{mask})	0.5
<i>Expression Encoding</i>	
Raw hidden dimension	512
Hard binning bins	50
Soft binning bins	20
Soft binning hidden dimension	512
Log binning max bins	10
<i>Other</i>	
Random seed	777
Number of data workers	8

A.2 HYPERPARAMETERS

Table 1 summarizes the hyperparameters used for training all models in this study. These hyperparameters were based on previous works (Cui et al., 2024; Adduri et al., 2025; Pearce et al., 2025).

A.3 TRAINING DATASETS

Table 2 lists all 101 training datasets used in this study, including the dataset identifier and number of cells for each dataset. The total number of cells across all training datasets is 10,010,835.

A.4 ADDITIONAL FIGURES

Table 2: Training datasets used for model pretraining. Dataset IDs are UUIDs from the curated dataset collection.

Dataset ID	Cells	Dataset ID	Cells	Dataset ID	Cells
7d98cc44-b090-4dc8-804f-2750c84fe9d7	2,489	2f05ab20-a092-4bab-9276-3e0eb24e3fee	38,217	3966ba97-beb8-4d0b-9954-d3775cd2cd61	158,978
2d66790a-6621-4a49-f8fd-4002db5cc98d	4,992	76150f40-1989-4977-9c23-696e72d59d9e	118,672	28ab6eb8-dfa4-4536-9f26-7e06c1b98e8e	25,741
50c4a6d6-940b-4c6a-a376-aea2e2d3168	21,003	c2a461b1-0c15-4047-9fcf-1966fe55100	97,499	c838aec3-03ef-4398-b882-0e3912abff0	1,265,624
cda2c8cd-be1c-42e5-b2cd-162caa1c4ce7	255,901	e40c6272-af77-4a10-9385-62a398884f27	65,088	3a29c3df-b45a-403d-bd76-259640245432	4,992
19e46756-9100-4e01-8b0e-23b557558a4c	66,985	ed11cc3a-2947-407c-883c-c53b0e3917c3	8,573	61d327d1-2227-4cf6-9367-e3559dc79b07	796
70e4f35b-c98c-45a1-9aa1-2053b07315d0	40,815	15327a6-7978-4896-ba91-69d6b402dbbf	40,191	eeac0c1-2217-4cf6-b8ce-1f0fedfb1b569	9,337
c5ac3ec2-24b0-43cc-9aa8-bb0ebe205ce	4,992	ad046b15-a095-43b0-9fb5-b36998d87fdb	4,992	0fe5eed4-bcbc-4c00-a388-00bc1455a9b7	4,992
bac09168-940b-4b11-8d55-b495f80b98d	12,461	9fcfac8d-bff6-47a2-a1f6-503827d375f5	637	43aa19d2-c723-4822-979d-d2f0239835e0	37,121
095940cb-7422-4510-96e2-cba9d961eb88	52,045	30f5e171-83d7-4fc0-bf75-384f122346b3	1,790	3079e9b0-c6db-45c8-b998-a4555a73968e	28,943
79884ac5-e026-4d44-8585-e807960bd477	4,425	489318a0-24c3-4fc5-b105-08f4ed0ea026	13,900	0920cb8c-4b3a-4e9d-a553-561529fd3b32	48,478
d551b400-b2e5-454d-b5a9-ece03e6b4739	4,992	a7b4f565-691d-43ea-bf4a-d2d1d5b2b4b4	27,111	93091496-be48-4122-b945-9a9c227535	28,718
b9b592d4-a0c0-4694-8704-a625289ef1f	4,992	34229bd8-a995-4394-8820-574e028d8c6	31,924	01209dce-3575-4bed-b1d1-129f571bc031	51,876
311657dc-1875-4c4b-a5ca-se63b3ef3a82	121,916	e5f5d954-cf0e-4b8d-9346-81ddf15a08b	2,487	879bb6df-cc2a-40f1-854b-5be9629d03b2	4,992
edbf0404-f1dd-496a-8237-df11d70621ca	77,525	06ef6b36-6c9b-4e10-8a94-d0ba7247276e	10,533	79527108-1f6c-4152-afe0-1fcdf2e02ba3	4,992
6f0858c0-c590-4740-b022-c152e7608d66	4,992	9ea768a2-87ab-46b6-a73d-c4e9152f5af3	40,268	dee75ca4-8348-471e-bbeb-e2143209e3d0	4,992
949e7fc-ac54-47e9-bb6f-ee967688ce	38,937	0bae7ebf-eb54-4f6b-be9a-3461ceef4ac	27,675	1df5fa02-4a0e-4b00-a203-cb0a60e75637	4,992
7291f397a-0812-4b52-a7d1-b377107ffb41	4,992	53d62b10-bae5-48ac-b16c-71be9ba6e59	4,992	364bd0e7-f7fd-48ed-99c1-ac26872b1042	931,012
ae4552dc-e2ea-4467-b375-30ec7480f780	37,275	fe2479fd-daff-41a8-97dc-a50457ab1871	292,010	50eb1c23-b8d4-4f76-a184-44e55416a05a	4,775
77c1c78-8094-4065-8c94-6a070783256	37,767	49108ba9-1b7a-4a8a-9859-3d3e0ba83926	4,992	39ed7d98-676d-4b8d-9d0d-0f3b60914ead	118,647
dd03ce70-3243-4c96-5611-330cc4164d7	23,732	00ba8341-48ec-4b5e-4a0d-0dd2d7913	4,992	9ddea8d9-c4c4-420a-90f6-880996808d4	100,307
9dbab10c-118a-496b-966a-671f763a6b7d	1,462,702	ca421096-6240-4cce-8c12-d20899b3e005	81,736	731e6380-879f-4b0b-9a1f-2150208852ef	2,065
43245158-5ae1-4e71-a9a6-67ef49c26bc	113,304	f801b7a9-80a4-6d09-9161-71474deb58a	6,044	54801477-ac3e-47e3-8170-96c5b40d5c10	4,992
43848156-ba94-47b5-8409-7535cea75678	4,992	c5ca2b7-abb1-4a50-9087-707b54ca606b	14,094	1cf24082-59de-4029-ac81-6e398768af3a	29,522
978a566a-dc27-478d-b306-26dab1161f	1,102,250	726afad9-df7b-4b56-967a-0fb79d85ee4b	4,992	9adbf1b29-65a2-4dd0-86bf-f02690d65fb	4,992
e6361237-ac4e-4c5d-ad8f-f16aca00a8f1	66,719	344f27ab-428c-4a0e-a7e1-d4441f2fb80	4,992	a18b241a-c72c-4470-b1a4-80e7336c6ab6	4,335
346c5aad-b034-4248-8c8e-0a05fd634b9c	163,779	529b209-9d7b-44da-bfa4-f6e474546c2	32,678	33da10b0-9c1d-4c82-9b14-67cdcf9fae5	30,022
d98e49fe-b70d-4434-8050-bb179b66e	15,216	5e57cd50-8e42-42d6-940d-5c1660d06864	693,682	3e55180c-780a-4424-9434-5296640fc0d	7,774
f3c49918-4707-4d92-bb6d-5c5dbbb8-1b4	15,177	c5cd6bbb-8ba4-4338-8b34-51ed52312e	4,992	b617ce1b-18c8-4d89-b82b-e803ab93550d	391,963
9f499d32-400d-4c42-a9a2-fb1481844fe	56,367	93131426-0124-4a84-a013-9dfb99d467	24,327	ab8896c6-f60a-4fb4-924e-ee19dcf909b	4,992
2f6a4db1-173d-4b8d-860b-c47fea120fa	2,868	75548d10-160d-4b8c-b317-99ad9630c62d	4,992	e84f2780-518c-4f8a-8a0-13bfe677c7	167,598
be401db3-1732-408a-b0c4-71af0458bab8	135,462	6e92c364-02e1-455a-840b-4fbceef132ae7	4,992	639ffcc2-14db-4060-9027-3c903142008	35,290
4724c395-0c46-46d2-8117-60fd271fb488	35,350	4f2de279-ab3a-4827-a773-1b7dcd099307	4,992	c775e88-49bf-4ba2-a03b-93f00447c958	647,366
155c186-df92-4b17-a253-199e10ffece08	4,992	019e7af2-c827-4454-9970-44d5c39ce068	12,590	842cf0d-0b0a-46d5-910c-fc833d83c45e	65,662
1b767195-d0a0-4a3d-b394-cc665d86c3dc	34,933	b3c55d0d-4529-4b61-b485-29026be04e	4,992		

Total: 10,010,835

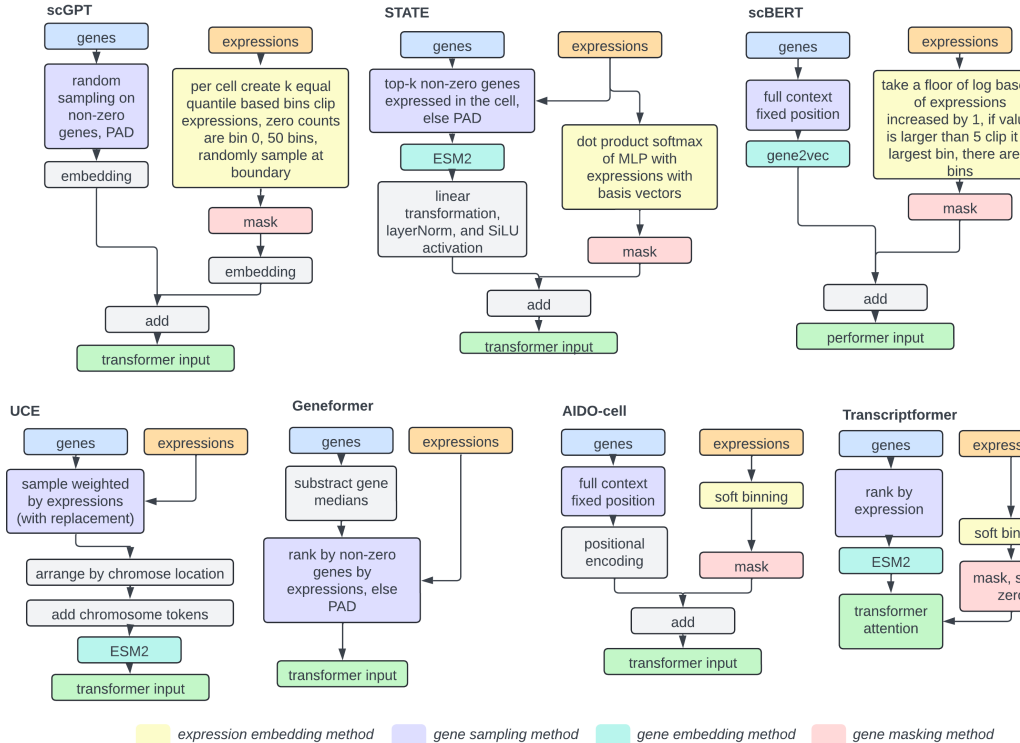


Figure 4: Schematic comparison of different gene and expression encoding methods across single-cell foundational models (Cui et al., 2024; Adduri et al., 2025; Ho et al., 2024; Wang et al., 2021; Theodoris et al., 2023; Pearce et al., 2025; Rosen et al., 2023).